3-1-2006

NMR Studies of Escherichia Coli Acyl Carrier Protein: Dynamic and Structural Differences of the Apo- and Holo-forms

Yangmee Kim
Konkuk University

Evgueni Kovriguine
Marquette University, evgueni.kovriguine@marquette.edu

Ziad Eletr
University of Georgia

Accepted version. *Biochemical and Biophysical Research Communications*, Vol. 341, No. 3 (March 2006): 776-783. DOI:

Biochemical and Biophysical Research Communications, Vol. 341, No. 3 (March 2006): 776-783. DOI.

Yangmee Kim
Department of Chemistry and Bio/Molecular Informatics Center, Konkuk University, 1 Hwayang-dong, Kwangjin-gu, Seoul 143-701, Republic of Korea

Evgenii L. Kovrigin
Department of Chemistry, Yale University, P.O. Box 208107, New Haven, CT 06520, USA

Ziad Eletr
Complex Carbohydrate Research Center, University of Georgia, 220 Riverbend Road, Athens, GA 30602-4712, USA

Abstract

Two indicators of conformational variability of Escherichia coli acyl carrier protein (ACP) have been investigated, namely backbone dynamics and chemical shift variations of ACP. Hydrophobic interactions between the 4'-PP prosthetic group and the hydrophobic pocket enclosed by the amphipathic helices resulted in chemical shift perturbations in the residues near the prosthetic group binding sites and contact sites in the hydrophobic pockets upon conversion from apo- to holo-forms. At pH 7.9, destabilization of ACP due to negative charge repulsions and the deprotonated state of His 75 resulted in observed chemical shift changes in the C-terminal region. Model-free analysis showed that the $\alpha_1\alpha_2$ loop region near the prosthetic group binding site in ACP shows the greatest flexibility (lowest S^2 values) and this result may suggest these flexibilities are required for structural rearrangements when the acyl chain binds to the prosthetic group of ACP. Flexibility of ACP shown in this study is essential for its ability to interact with functionally different enzyme partners specifically and weakly in the rapid delivery of acyl chain from one partner to another.

Keywords

Acyl carrier protein, Hydrophobic interaction, Metal binding, Chemical shift, Dynamics

Introduction

Acyl carrier protein (ACP) is a small (~9 kDa) acidic protein whose function is essential for numerous biosynthetic pathways that depend upon acyl group transfer. The structures of several acyl carrier proteins have been solved by solution NMR and X-ray crystallography [1], [2], [3], [4], [5]. The overall structure consists of four α-helices (helix I (3–15), helix II (37–51), helix III (56–61), and helix IV (65–75)) connected by three loops. The crucial prosthetic group and acyl chain carrying residue, Ser36, is located at the junction of the $\alpha_1\alpha_2$ loop near the N-terminal region of helix II. However, relatively little data on the dynamics of the structure and the changes which occur on introduction of the prosthetic group exist. We provide some of those data here.

The predominant role of ACP in Escherichia coli is in the biosynthesis of fatty acids. To function in this regard, inactive apo-ACP is first converted to the active holo form by the enzyme ACP-synthase, which catalyzes the transfer of 4′-phosphopantetheine group (4′-PP) of coenzyme A to the γ-OH group of the strictly conserved residue, serine 36, through the formation of a phosphodiester linkage. Acyl groups are activated for transfer to the growing lipid chain through thioester bond formation with the terminal cysteamine group of 4′-PP-ACP (holo-ACP). Activated ACP then interacts with other members of the fatty acid synthase pathway so that 2-carbon units are added to the beginning of the growing acyl chain. In prokaryotes, the biosynthesis of fatty acids is accomplished by individual enzymes whereas in mammalian fatty acid synthesis the task is achieved by large multifunctional enzymes. In prokaryotes, protein: protein interactions are necessary for fatty acid production. therefore, disruption of these interactions is the subject of therapeutic efforts.

Acyl carrier proteins also function in a variety of other processes that require acyl transfer steps such as synthesis of polyketide antibiotics [6], lipopolysaccharides [7], rhizobial nodulation signaling factors [8], lipoteichoic acids [9], as well as prohemolysin toxin activation [10]. In addition, ACP is required for glucosyltransfer in a 4′-PP independent process [11]. It is therefore essential for ACP to specifically interact with numerous proteins during the process of cell growth and distinct regions of ACP are known to be essential for proper biological function [5], [12], [13], [14]. Some of these regions must communicate information about functionalization of ACP's prosthetic group. However, structural studies indicate that at least the apo- and holo-forms of ACP are identical. Therefore, it is unclear how functional specificity is achieved. One possibility is that protein dynamics may play a role modulating specific protein interactions [15], [16], [17], [18], [19], [20].

Inherent flexibility in E. coli holo-ACP has been previously shown to account for inconsistent NOE constraints [21]. Furthermore, hydrogen–deuterium exchange experiments at pH 6.0 indicate rich ACP dynamics that portray helix II (residues 37–51) as the least stable of the secondary structure elements in the apo form [22]. These experiments additionally identified the C-terminal portion (residues 26–34) of the $\alpha_1\alpha_2$ loop as having greater protection factors than residues at the N-terminal region (residues 15 and 17) of this loop. NMR and X-ray studies of the homologous Bacillus subtilis ACP suggest that the $\alpha_1\alpha_2$ loop becomes ordered and populates helical conformational space upon binding to ACP synthase [2], [5]. The frenolicin holo-ACP, which shares 21% sequence identity to the *E. coli* form, exhibits extensive mobility (low NMR order parameters, S^2) in the $\alpha_1\alpha_2$ loop and the C-terminal residues (56–63) exhibit a slow conformational exchange process [4]. Thus, a myriad of dynamics appear throughout the ACP family of proteins, perhaps reflecting their functional plasticity.

Flexibility is believed to be essential for the ability of ACP to interact with multiple enzyme partners and undergo conformational changes as its reversibly directs acyl groups to the active sites for these enzymes. There are two important factors that could influence the conformational stability of E. coli ACP. First, ACP can have hydrophobic interactions between the various acyl moieties of the modified 4′-PP prosthetic group and the hydrophobic pocket enclosed by the amphipathic helices [23], [24]. Second, ACP is highly acidic protein, therefore solution pH or the binding of divalent cations at discrete sites on the protein can neutralize the repulsive effects of the 20 acidic residues in ACP and result in its conformational stabilization [25], [26], [27], [28]. Here, we investigated the factors that can influence the conformational stability of *E. coli* ACP through observation of backbone dynamics changes and chemical shift variation of ACP.

Experimental procedures

Expression and purification of *^{15}N-labeled ACP.* The cDNA of E. coli acyl carrier protein (ACP) was previously cloned [29] into a pET11a vector (Novagen) containing an IPTG inducible promoter and resistance to ampicillin. ^{15}N-labeled ACP was produced in 1 L M9 minimal media supplemented with 100 µg/ml ampicillin and 1 g/L $^{15}NH_4Cl$ (Cambridge Isotope Laboratories). Purification of ACP follows methods previously described [29], [30]. Mixed apo- and holo-ACP was converted entirely to the holo-ACP using the crude synthase isolated directly from a cation exchange column and coenzyme A (Sigma, St. Louis, MO) as described previously [31]. NMR samples were dialyzed against 25 mM Mes buffer, pH 6.1, containing 5 mM DTT and 5 mM $CaCl_2$.

NMR experiments. All protein NMR experiments were performed on 1 mM ^{15}N-labeled apo-ACP and 0.5 mM ^{15}N-labeled-ACP samples using a 3-channel Varian Unity+ 600 MHz instrument and a Z-gradient equipped Varian HCN probe located in the Yale University Chemical Instrumentation Center. Typically, 40 µs ^{15}N 90°-pulse widths were achievable with this probe. The experimental temperature was calibrated to 298 K using a 100% methanol standard. Ambiguities in resonance assignments were resolved by recording a ^{15}N-edited NOESY-HSQC [32], [33] and ^{15}N-edited TOCSY-HSQC [34]. NMR spin-relaxation experiments were performed using published, gradient-selected sensitivity-enhanced pulse sequences [35], [36], [37]. The longitudinal (R_1) spin-relaxation rates were measured with relaxation delays of 0.0 (×2), 0.112, 0.222, 0.352 (×2), 0.532, 0.802 s. The transverse (R_2) relaxation rates were obtained with 1.0 ms spacing between ^{15}N 180° CPMG pulses at total relaxation delays of 0.0 (×2), 0.02, 0.04, 0.076, 0.124 (×2), 0.184, 0.284 seconds. For R_2 measurements, temperature-compensating ^{15}N 180° pulses were applied during the recycle delay [38]. The heteronuclear cross-relaxation rate (NOE) was obtained by interleaving pulse sequences with and without proton saturation. All relaxation spectra were acquired with the ^{1}H carrier set coincident with the water resonance and ^{15}N frequency set to 118 ppm; spectral widths were 7000 and 2000 Hz in the t_2 and t_1 dimensions with 2048 and 120 complex points in each dimension, respectively. A recycle delay of 2.5 s was used in all (R_1, R_2) relaxation experiments. NMR data were processed with NMRPipe [39] and visualized with Sparky [40]. Longitudinal and transverse relaxation rates were determined by fitting the peak heights (obtained from a 3 × 3 grid located at the peak maxima) to a single exponential decay by a non-linear least-squares routine using in-house written software and the program 'Curvefit' provided by Professor Arthur G. Palmer (http://cpmcnet.columbia.edu/dept/gsas/biochem/labs/palmer/software.html). The heteronuclear NOE was determined from the ratio of peak heights for experiments with and without ^{1}H-saturation pulses.

Model-free analysis. Protein amide backbone dynamics were characterized by fitting NMR spin-relaxation rates to 1 of 5 semi-empirical forms of the spectral density function using the model-free formalism [41], [42].

The five models used to describe the spin-relaxation data are described according to their corresponding free parameters in the following equation (1)[44]:

$$\begin{aligned} &\text{Model1}{:}S^2 \\ &\text{Model2}{:}S^2,\tau_e, \\ &\text{Model3}{:}S^2,R_{ex}, \\ &\text{Model4}{:}S^2,\tau_e,R_{ex}, \\ &\text{Model5}{:}S_f^2,S^2,\tau_e, \end{aligned} \qquad (1)$$

in which τ_e is the internal correlation time, S^2 is the generalized order parameter, is the order parameter for fast motion, with a typical correlation time <10 ps, and R_{ex} is the additional linebroadening due to assumed, two-site conformational exchange and depends on the equilibrium site populations, the chemical shift differences, and the rate of exchange between conformers. Fitting of motional parameters to the spin-relaxation data was performed using the selection method described for the program FAST-Model-free [44] interfaced with 'Model-

Free 4.01' [43], [45]. Model selection was based on the statistical testing protocol described previously by Mandel et al. [43]. The rotational diffusion tensor for ACP was estimated from R_2/R_1 ratios and the program 'R2R1_diffusion' using the solution coordinates, (1ACP) and the program 'pdbinertia' (provided by Professor Arthur G. Palmer). The criteria for inclusion of residues in the diffusion tensor estimate relied on the method of Tjandra et al. [46]. During the model-free analysis, an axially symmetric rotational diffusion tensor was used, the N–H bond lengths were assumed to be 1.02 Å, and the ^{15}N chemical shift anisotropy was assumed to be −160 ppm [47], [48]. For each model, 300 randomly distributed data sets were generated. Models were selected by comparing the sum-squared error of the optimal fit with the 0.05 critical value of the distribution. In cases where *F*-statistics were applicable, comparisons were made with the 0.20 critical value of the distribution.

Results and discussion

Solution NMR experiments

^{15}N-labeled acyl-carrier protein (ACP) in the apo- and holo-forms was expressed and purified. The two-dimensional ^{1}H–^{15}N HSQC spectra at pH 5.9 and 7.9 for the apo- and holo-forms of ACP are shown in Fig. 1. Using previous resonance assignments for apo-ACP [29] and TOCSY- and NOESY-HSQC experiments acquired at 14.1 T, a total of 74 out of 76 non-proline backbone residues could be assigned at pH 5.9 for the apo- and holo-forms, and 74 residues at pH 7.9 for both forms. Fig. 1 shows overlays of HSQC spectra at both pH values for the holo and apo forms. The typical fraction of the non-phosphopantetheine form of ACP (apo-ACP) obtained from protein preparations is 80% with the remainder being holo-ACP (20%). The relative amount of apo:holo proteins in the apo-ACP sample determined by a 1D trace through the ^{15}N dimension for residue Leu37 is ~80% apo and ~20% holo forms.

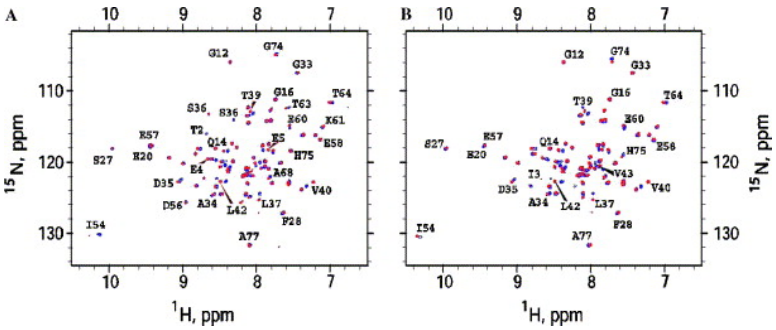

Fig. 1. NMR spectra of ACP. (A,B) Overlay of two-dimensional ^{1}H–^{15}N HSQC spectra of the apo (blue) and holo (red) forms of ACP. Spectra were acquired at pH 5.9 (A) and pH 7.9 (B). Peaks were assigned using a combination of ^{1}H–^{15}N NOESY-HSQC and ^{1}H–^{15}N TOCSY-HSQC and are shown using the one-letter amino acid code.

Previous NMR studies on ACP have shown that the apo- and holo-forms of these proteins are essentially identical and no NOEs between the prosthetic group and holo-ACP residues are detected unless ACP is acylated [1], [3], [23], [24]. Based on ^{19}F–^{1}H heteronuclear nuclear Overhauser studies of acyl chain-binding site of ACP, ^{19}F located at the 5-position of the acyl chain is in close contact with the protein primarily through interactions with Ile54 and Ala59 [23].

To assess the effects of covalent attachment of the prosthetic group to ACP, the backbone ^{15}N and ^{1}H^{N} chemical shift variations upon conversion of the apo form of ACP to the holo state were investigated. These changes in backbone chemical shifts calculated by the method of Wuthrich and co-workers [49] are depicted in Fig. 2. Deviations are small for most of the residues and suggest that the structures of apo-ACP and holo-ACP are almost identical. However, the residues near the prosthetic group binding site show chemical shift perturbations. At pH 5.9, residues from Asp35 to Met44, which are near the site of prosthetic group attachment, undergo significant chemical shift changes. Also, Ile54, Glu60, Ile62, and Ala68 show chemical shift variations between two forms. The side chains of these residues, with the exception of Glu60, are located in a hydrophobic

cleft that is purported to provide interactions with the prosthetic group. The sites of 4'-PP induced chemical shift changes at pH 5.9 are mapped onto the structure of ACP (Fig. 3A). The crystal structure of butyryl-ACP I62M where Ile62 was substituted with Met62 shows that the terminal methyl group of the butyryl moiety is located in a pocket lined by the side chains of residues Val7, Leu46, Ile54, Met62, Tyr71, and Ile72 [50]. The mercaptoethylamine moiety in the 4'-PP prosthetic group is stabilized by a hydrogen bond between its amide nitrogen atom and the main chain carbonyl group of Glu60. As shown in Fig. 2, Fig. 3, Glu60 shows the chemical shift variations between apo- and holo-forms. At pH 7.9 (Fig. 2B), the pattern of chemical shift changes between the apo-and holo-forms is similar to those seen at pH 5.9. These results suggest that while the structures of the apo- and holo-forms are very similar, the prosthetic group transiently interacts with residues in the hydrophobic cleft resulting in a perturbation of their chemical shifts. It has been reported that ACP from Mycobacterium tuberculosis also shows similar prosthetic group dynamics [51].

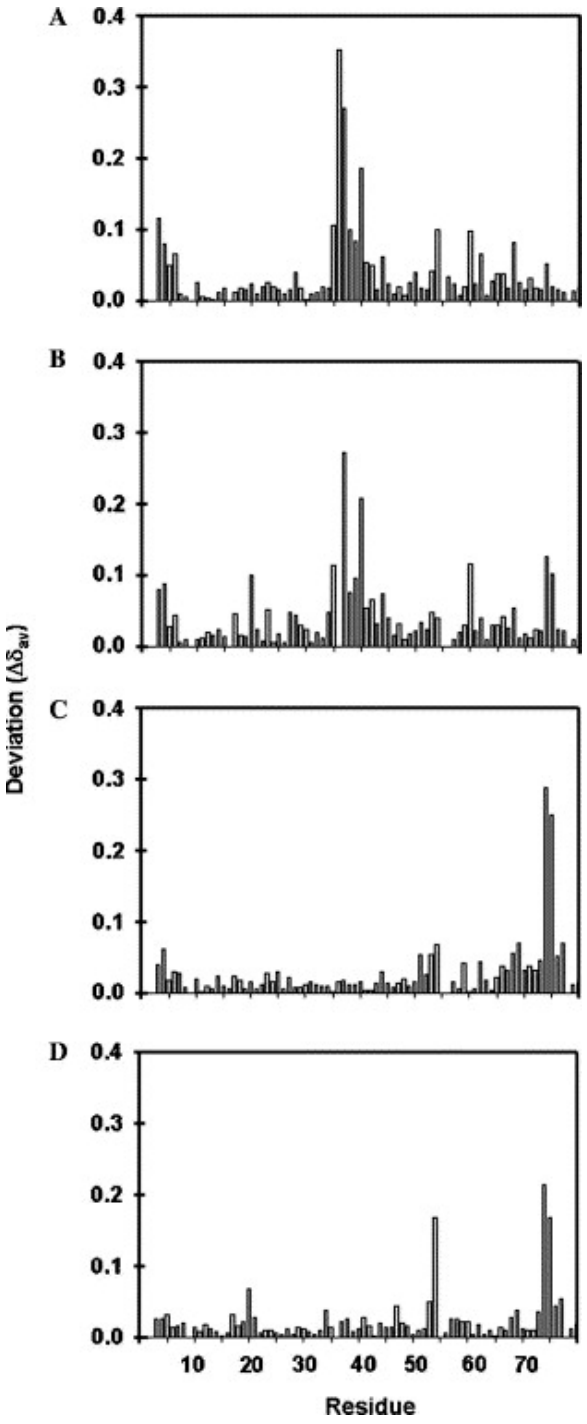

Fig. 2. Chemical shift changes in ACP induced by phosphopantetheine modification and elevation of pH. (A) The deviation between holo- and apo-ACP at pH 5.9. (B) Deviation between holo- and apo-ACP at pH 7.9. (C) For holo-ACP, the deviation between pH 5.9 and 7.9 samples and for (D) chemical shift deviation for apo-ACP between pH 5.9 and 7.9. $\Delta\delta_{av} = \{0.5[\Delta\delta\ (^{1}H^{N})^{2} + (0.2\Delta\delta\ (^{15}N))^{2}]\}^{1/2}$ [49] where $\Delta\delta\ (^{1}H^{N})$ and $\Delta\delta\ (^{15}N)$ are the chemical shift differences for the $^{1}H^{N}$ and ^{15}N atoms between apo- and holo-forms [49].

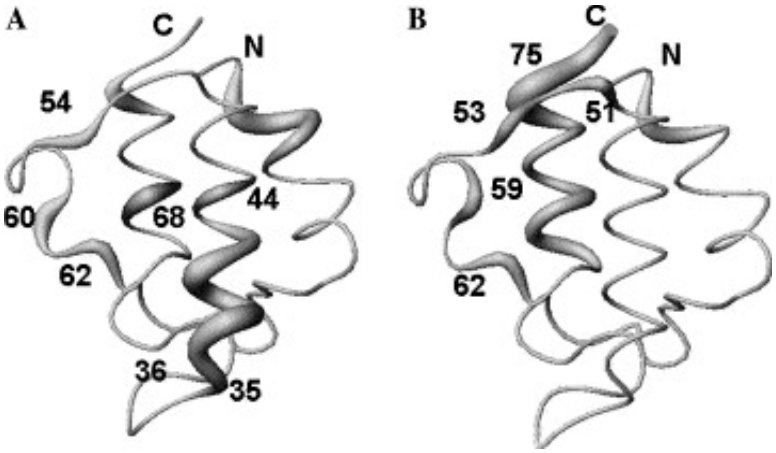

Fig. 3. Spatial representation of chemical shift changes in ACP induced by phosphopantetheine modification and elevation of pH. The changes in chemical shift shown in Fig. 2 are mapped onto a worm representation of ACP. (A) The thickness of the worm is proportional to the chemical shift changes between the holo- and apo-ACP at pH 5.9 and reflects the magnitude, $\Delta\delta_{av}$, of chemical shift changes upon covalent linkage between Ser36 and the phosphopantetheine prosthetic group. (B) The thickness of the worm is proportional to the chemical shift changes of holo-ACP between that at pH 5.9 and that at pH 7.9. The figure was prepared with MolMol [55].

It is well known that fatty acid synthesis is stimulated by the addition of divalent cations that give rise to ion-induced changes in the structure of ACP [11]. Two sites, each capable of binding Mg^{2+} or Ca^{2+}, have been proposed [25], [26], [27], [28]. Manganese paramagnetic effects, identified using the T_1-accordian COSY experiment, have identified two ion-binding sites on the protein [28]. These sites appear to cluster around two distinct well-separated regions involving E30 (site A) and E48 (siteB), respectively. Site A appears to utilize E30, D35, and D38 in its ion coordination. Site B is near a proline-containing bend and appears to involve stronger interactions with acidic residues, E47, D51, E53, and D56. Mn(II) EPR-binding studies with holo-ACP also suggested the presence of two high affinity metal-binding sites at physiological pH [25].

In order to investigate the effects of solution pH on the structure of ACP, the backbone ^{15}N and $^{1}H^{N}$ chemical shift variations at pH 5.9 and at pH 7.9 for holo-ACP and apo-ACP were analyzed. As shown in Figs. 2C and D, the effects of pH on the apo- and holo-proteins are similar. The largest pH effects are localized to the C-terminal region and to residues 50–60. Fig. 3B shows the change in chemical shifts at low and high pH for the holo-ACP. The pH-dependent chemical shift variations occur in the C-terminal helical region, which includes His75, Ala59 located in helix III, and Ile62 located in the loop joining helices III and IV as well as residues comprising the consensus metal-site B. In contrast, Site A does not show any variations in chemical shift with pH. These studies indicate that the predominant pH effects are manifest near the C-terminus of ACP and in residues surrounding metal-site B. CD spectroscopic analysis of the effect of Mg^{2+} on the ACP structure showed that the native ACP conformation can be stabilized by divalent cation [26], [27], [52]. The imidazole side chain of His residue has a pK_a value near 6–7 and it is one of the strongest bases at neutral pH. Therefore, not only divalent cation but also His 75 at C-terminus of ACP can stabilize the electrostatic repulsion between the acidic residues at neutral pH. However, at high pH, the imidazole ring becomes a much weaker base and His 75 cannot prevent loss of secondary structure that occurs due to electrostatic repulsion of acidic residues at elevated pH. Consequently, destabilization of these regions of ACP could result in the observed chemical shift changes between two different pH 5.9 and 7.9.

To further investigate the origins of the pH-dependent chemical shift changes, NMR spin-relaxation measurements were performed. Longitudinal (R_1) and transverse (R_2) relaxation rates and the heteronuclear NOE were measured. Because there are relatively few changes in chemical shifts upon conversion of apo- to holo-ACP, the NMR spin-relaxation rates for a majority of the residues for the 'contaminated' apo-ACP sample

will be a population-weighted average of the two forms. For this reason a quantitative assessment of dynamics will be restricted to holo-ACP at pH 5.9 and 7.9 where this contamination has little effect.

The results of the spin-relaxation experiments are shown in Fig. 4. There are minor effects of pH on the spin-relaxation rates. The average (10% trimmed) R_1, R_2, and NOE values at pH 5.9 and 7.9 (henceforth unless specified all discussion will concern the holo form), respectively, are 2.10 ± 0.06, 6.44 ± 0.25, 0.790 ± 0.096, 2.02 ± 0.07, 6.92 ± 0.18, and 0.734 ± 0.079 s^{-1}. The relaxation rates in ACP show relatively uniform behavior across the protein sequence with the exception of loop regions, including Glu53 and residues at the C-terminus. In addition for holo-ACP, relaxation data are obtained for both NH groups in the 4'-PP moiety; these are also shown in Fig. 4, indicated as positions 79 and 80. The significantly reduced relaxation rates for NH groups in the prosthetic group compared to those of the protein backbone are consistent with 4'-PP being very mobile and making few long-lived interactions with ACP (vide supra). Because the NH group of Glu53 is very close to that of the mercaptoethylamine moiety in the 4'-PP prosthetic group, the distinct relaxation behavior of Glu53 may be caused by the transient interactions with this region of the prosthetic group.

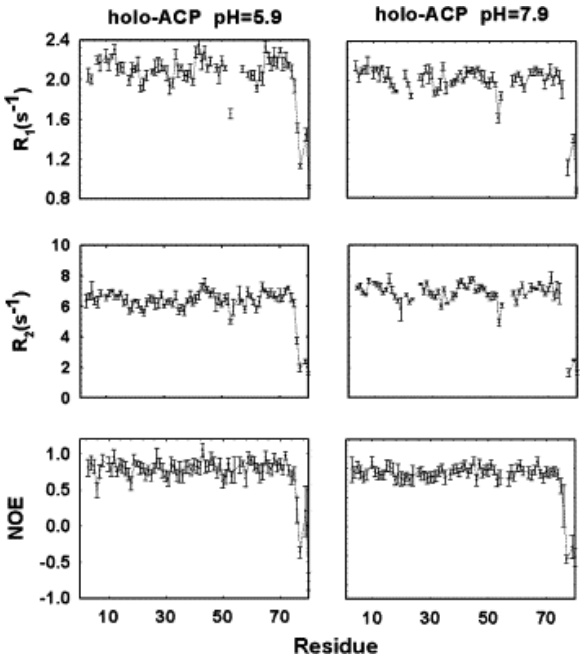

Fig. 4. Summary of NMR spin-relaxation results. NMR data are displayed as a function of ACP amino acid residue for the holo-form at pH 5.9 and pH 7.9. Breaks in the lines indicate regions of missing data as a result of proline, data peak overlap or data of inadequate *S*/*N*. The two data points at position 79 and 80 represent relaxation data for the NH groups of the phosphopantetheine moiety.

NMR-derived dynamics parameters

Model-free analysis was performed as described [43] to obtain global and site-specific dynamics information. Using an axially symmetric diffusion tensor, the rotational correlation time, τ_m, was found to be 4.40 ± 0.06 and 4.79 ± 0.06 ns at pH 5.9 and 7.9 with $D_{\parallel}/D_{\perp}$ = 0.86 and 0.84, respectively. These values are in agreement with theoretical predictions based on the molecular mass of ACP and from hydrodynamic calculations [53]. In addition, the order parameter, S^2, describing the degree of spatial restriction of the backbone NH bond vector was determined by model-free analysis and is shown in Fig. 5. The backbone dynamics for the majority of amino acid residues are best described by model 1. At pH 5.9, 58 residues are best fit by model 1, 2 residues are fit to model 2, 2 to model 3, and 1 (Ala77) to model 5. At pH 7.9, 52 residues are best described by model 1, 1 (Val18) by model 2, 6 by model 3, and 1 (Ala77) by model 5. The average S^2 values for the entire protein (10% trimmed) determined at pH 5.9 and 7.9 are 0.862 ± 0.020 (63 quantifiable residues) and 0.864 ± 0.014 (61 quantifiable

residues). The overall results indicate that: (1) there are minimal quantitative overall differences in the equilibrium fluctuations of the backbone NH groups of ACP at the two pH values and (2) the site-specific pattern of S^2 values does not show a pH dependence. The centers of loop regions in ACP show the greatest flexibility (lowest S^2 values) which decreases nearer to the α-helices. Likewise the helix regions show increased flexibility at the ends where the helix enters and exits the intervening loops, while the center of helix shows the greatest rigidity. The backbone dynamics of an ACP (fren holo-ACP) involved in polyketide biosynthesis have been characterized [4]. This protein has little sequence identity (21%) to E. coli ACP studied here yet the overall helix topology of the two proteins is similar. Functionally, fren holo-ACP is able to interact with the *E. coli* holo-ACP synthase [54]. Yet, the overall backbone rmsd is ~3 Å for the two proteins. The S^2 values for fren holo-ACP are also high except in loop I, which connects helices I and II. Similarly, in the case of *E. coli* ACP, residues in $\alpha_1\alpha_2$ loop which connects helix I and helix II show great flexibility.

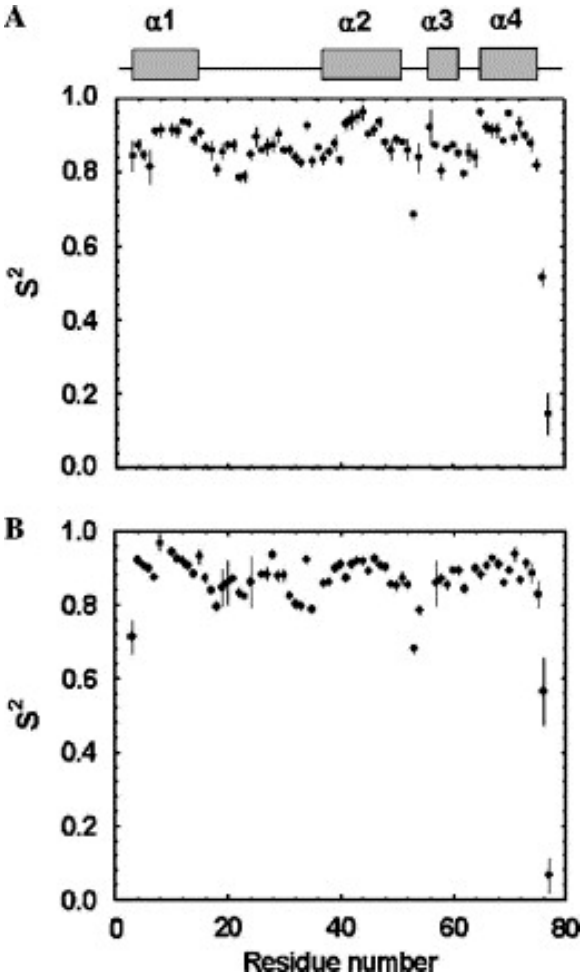

Fig. 5. NMR order parameters. Values of S^2 are shown versus ACP amino acid sequence for the holo form (A) at pH 5.9 and (B) pH 7.9. Breaks in the lines indicated regions of missing data as a result of proline, data peak overlap, inadequate *S*/*N*, or residues in which no motional model could be fit. Secondary structure is shown above the data plot with rectangles indicating α-helical regions.

Slower timescale (μs–ms) motions are also captured from the model-free analysis. These conformational exchange motions result in additional linebroadening (R_{ex}) of the NMR signal. The pattern of exchanging residues in ACP shows slight pH dependence. At pH 5.9, Thr64, Asn73, and Gln 76 near His 75 are in chemical exchange. At pH 7.9, the exchanging residues are Ala26, Leu32, and Met44. These latter residues are in the $\alpha_1\alpha_2$ loop or in the second α-helix. Order parameters, S^2, are colored onto the ribbon structure of holo at pH 5.9 and 7.9 in Fig. 6. The values of R_{ex} for the residues greater than 0.5 s^{-1} are shown with a larger ribbon diameter. In addition at

pH 7.9 there are two other residues that have R_{ex} values slightly smaller than 0.5 s^{-1}. They are Val40 and Glu41. It is interesting to note that they spatially cluster near residues with more significant R_{ex} values.

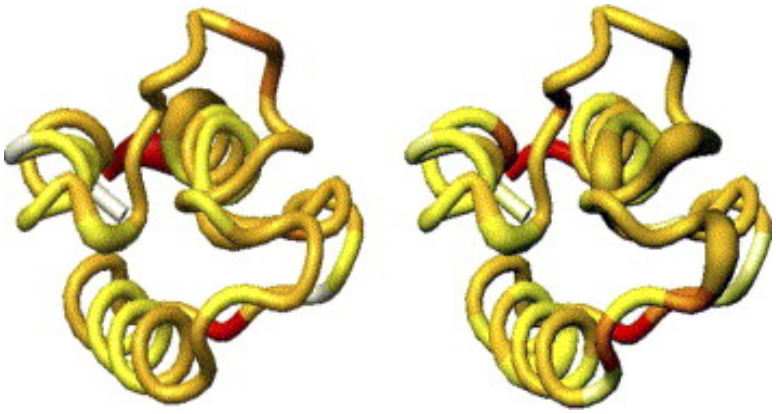

Fig. 6. Spatial location of NMR-derived dynamical parameters. Order parameters, S^2, are colored onto the tubular drawing of holo at pH 5.9 and 7.9. The color scheme is red ($S^2 < 0.70$) and yellow ($S^2 > 0.90$). For values $0.80 < S^2 < 0.90$, residues are colored from orange to yellow in a linear fashion. Residues with $R_{ex} > 0.5$ s^{-1} are shown with larger ribbon diameter. The figure was prepared with MolMol [55].

Conclusion

ACP is believed to be a mobile protein and flexibility is believed to be essential for its interaction with functionally different enzyme partners and conformational changes which facilitate the entry and exit of acyl groups attached to the prosthetic group from the active sites of these enzymes. In this work, observations point to two important factors that can influence the conformational stability of E. coli ACP. The effects of solution pH on ACP chemical shift variations and spin-relaxation data of holo-ACP point to electrostatic interactions which can also modulate stability. Hydrophobic interactions between 4'-PP prosthetic group and the hydrophobic pocket enclosed by the amphipathic helices can be the source of differences in the NMR data of holo-ACP and apo-ACP.

No significant differences in the backbone ^{15}N and $^{1}H^{N}$ chemical shift and NOE patterns were noted between apo- and holo-forms of ACP for most residues, suggesting that the structures of two forms are essentially the same. However, residues from Asp35 to Met44, which are near the site of prosthetic group attachment, undergo chemical shift perturbations. Ile54, Glu60, and Ile62 located in the segments between the second helix and the fourth helix show chemical shift variations between two forms and these residues are located in a hydrophobic cleft that is purported to provide interactions with the prosthetic group. These results suggest that while the structures of the apo- and holo-forms are very similar, the prosthetic group transiently interacts with residues in the hydrophobic cleft resulting in a perturbation of their chemical shifts. Low order parameters in this region and $\alpha_1\alpha_2$ loop as shown in Fig. 5 may imply the flexibilities that might be required for the structural rearrangements when the acyl chain binds to the prosthetic group of ACP.

In order to investigate the effects of solution pH on the structure of ACP, the backbone ^{15}N and $^{1}H^{N}$ chemical shift variations and spin-relaxation data at pH 5.9 and at pH 7.9 for holo-ACP were analyzed. The largest pH effects are localized to the C-terminal region and to residues comprising the consensus metal-site B. Raising the pH would enhance negative-charge repulsion, thereby destabilizing the structure. His75 at the C-terminus is surrounded by negatively charged residues such as Glu4, Glu5, Asp51, Glu53, and Glu58 as well as C-terminal carboxylate. It has been reported that partial positive charge of His 75 stabilizes the conformation of ACP in the C-terminal region [52]. However, at pH 7.9, destabilization of ACP due to electrostatic repulsion and the

different protonation state of His75 contribute to the pH-dependent stability of native state and result in the observed chemical shift changes in C-terminal region.

However, according to the ^{15}N nuclear spin-relaxation measurements on ACP, there are minor effects of pH on the spin-relaxation rates as a result of solution pH changes. There are minimal quantitative overall differences in the equilibrium fluctuations of the backbone NH groups of ACP at the two pH values and the site-specific pattern of S^2 values does not show a pH dependence. At both pH, each element of secondary structure in ACP has higher S^2 values than those of the loop regions. Model-free analysis showed that the $\alpha_1\alpha_2$ loop region near the prosthetic group binding site in ACP shows the greatest flexibility (lowest S^2 values) and this result may imply that these flexibilities are required for structural rearrangements when the acyl chain binds to the prosthetic group of ACP. Flexibility of ACP shown in this study could be essential for its interaction with different enzyme partners specifically and weakly to allow rapid delivery of acyl chain from one to another.

Acknowledgments

Y. Kim was supported by a Molecular and Cellular BioDiscovery Research Program Grant (M10301030001-05N0103-00110) from the Ministry of Science and Technology, and by grants from the Ministry of Science and Technology, Korea, and the Korea Science and Engineering Foundation through the Research Center for Proteineous Materials. We thank Professor J. Patrick Loria at Yale University and Professor J.H. Prestegard at the University of Georgia for useful discussions.

References

[1] T.A. Holak, S.K. Kearsley, Y. Kim, J.H. Prestegard **Three-dimensional structure of acyl carrier protein determined by NMR pseudoenergy and distance geometry calculations** Biochemistry, 27 (16) (1988), pp. 6135-6142

[2] G.Y. Xu, A. Tam, L. Lin, J. Hixon, C.C. Fritz, R. Powers **Solution structure of *B. subtilis* acyl carrier protein** Structure (Camb.), 9 (4) (2001), pp. 277-287

[3] Y. Kim, J.H. Prestegard **Refinement of the NMR structures for acyl carrier protein with scalar coupling data** Proteins-Struct. Funct. Genet., 8 (4) (1990), pp. 377-385

[4] Q. Li, C. Khosla, J.D. Puglisi, C.W. Liu **Solution structure and backbone dynamics of the holo form of the frenolicin acyl carrier protein** Biochemistry, 42 (16) (2003), pp. 4648-4657

[5] K.D. Parris, L. Lin, A. Tam, R. Mathew, J. Hixon, M. Stahl, C.C. Fritz, J. Seehra, W.S. Somers **Crystal structures of substrate binding to *Bacillus subtilis* holo-(acyl carrier protein) synthase reveal a novel trimeric arrangement of molecules resulting in three active sites** Struct. Fold. Des., 8 (8) (2000), pp. 883-895

[6] B. Shen, R.G. Summers, H. Gramajo, M.J. Bibb, C.R. Hutchinson **Purification and characterization of the acyl carrier protein of the *Streptomyces glaucescens* tetracenomycin C polyketide synthase** J. Bacteriol., 174 (11) (1992), pp. 3818-3821

[7] C.R.H. Raetz F.C. Neidhardt (Ed.), *Escherichia coli* and *Salmonella*: Cellular and Molecular Biology, American Society for Microbiology, Washington, DC (1996), pp. 1035-1063

[8] O. Geiger, H.P. Spaink, E.P. Kennedy **Isolation of the *Rhizobium leguminosarum* NodF nodulation protein: NodF carries a 4′-phosphopantetheine prosthetic group** J. Bacteriol., 173 (9) (1991), pp. 2872-2878

[9] M.P. Heaton, F.C. Neuhaus **Role of the d-alanyl carrier protein in the biosynthesis of d-alanyl-lipoteichoic acid** J. Bacteriol., 176 (3) (1994), pp. 681-690

[10] J.P. Issartel, V. Koronakis, C. Hughes **Activation of *Escherichia coli* prohaemolysin to the mature toxin by acyl carrier protein-dependent fatty acylation** Nature, 351 (6329) (1991), pp. 759-761

[11] H. Therisod, A.C. Weissborn, E.P. Kennedy **An essential function for acyl carrier protein in the biosynthesis of membrane-derived oligosaccharides of *Escherichia coli*** Proc. Natl. Acad. Sci. USA, 83 (19) (1986), pp. 7236-7240

[12] H. Gong, D.M. Byers **Glutamate-41 of *Vibrio harveyi* acyl carrier protein is essential for fatty acid synthase but not acyl-ACP synthetase activity** Biochem. Biophys. Res. Commun., 302 (1) (2003), pp. 35-40

[13] L.J. Tang, A.C. Weissborn, E.P. Kennedy **Domains of *Escherichia coli* acyl carrier protein important for membrane-derived-oligosaccharide biosynthesis** J. Bacteriol., 179 (11) (1997), pp. 3697-3705
[14] L.A.S. Worsham, L. Earls, C. Jolly, K.G. Langston, M.S. Trent, M.L. Ernst-Fonberg **Amino acid residues of *Escherichia coli* acyl carrier protein involved in heterologous protein interactions** Biochemistry, 42 (1) (2003), pp. 167-176
[15] P.A. Carr, H.P. Erickson, A.G. Palmer **Backbone dynamics of homologous fibronectin type III cell adhesion domains from fibronectin and tenascin** Structure, 5 (7) (1997), pp. 949-959
[16] K. Hilpert, H. Wessner, J. Schneider-Mergener, K. Welfle, R. Misselwitz, H. Welfle, A.C. Hocke, S. Hippenstiel, W. Hohne **Design and characterization of a hybrid miniprotein that specifically inhibits porcine pancreatic elastase** J. Biol. Chem., 278 (27) (2003), pp. 24986-24993
[17] W.L. Jorgensen **Rusting of the lock and key model for protein-ligand binding** Science, 254 (1991), pp. 954-955
[18] L.E. Kay, D.R. Muhandiram, G. Wolf, S.E. Shoelson, J.D. Forman-Kay **Correlation between binding and dynamics at SH2 domain interfaces** Nat. Struct. Biol., 5 (2) (1998), pp. 156-163
[19] M.G. Rudolph, T. Linnemann, P. Grunewald, A. Wittinghofer, I.R. Vetter, C. Herrmann **Thermodynamics of Ras/effector and Cdc42/effector interactions probed by isothermal titration calorimetry** J. Biol. Chem., 276 (26) (2001), pp. 23914-23921
[20] J.Y. Suh, L. Spyracopoulos, D.W. Keizer, R.T. Irvin, B.D. Sykes **Backbone dynamics of receptor binding and antigenic regions of a *Pseudomonas aeruginosa* pilin monomer** Biochemistry, 40 (13) (2001), pp. 3985-3995
[21] Y. Kim, J.H. Prestegard **A dynamic model for the structure of acyl carrier protein in solution** Biochemistry, 28 (1989), pp. 8792-8797
[22] M. Andrec, R.B. Hill, J.H. Prestegard **Amide exchange rates in *Escherichia coli* acyl carrier protein: correlation with protein structure and dynamics** Protein Sci., 4 (5) (1995), pp. 983-993
[23] P.J. Jones, E.A. Cioffi, J.H. Prestegard **[^{19}F]-1H heteronuclear nuclear Overhauser effect studies of the acyl chain-binding site of acyl carrier protein** J. Biol. Chem., 262 (1987), pp. 8963-8965
[24] K.H. Mayo, J.H. Prestegard **Acyl carrier protein from *Escherichia coli*. Structural characterization of short-chain acylated acyl carrier proteins by NMR** Biochemistry, 24 (1985), pp. 7834-7838
[25] D. Tener, K.H. Mayo **Divalent cation binding to reduced and octanoyl acyl-carrier protein** Eur. J. Biochem., 189 (1990), pp. 559-565
[26] A.S. Flaman, J.M. Chen, C.V. Iderstine, D.M. Byers **Site-directed mutagenesis of acyl carrier protein (ACP) reveals amino acid residues involved in ACP structure and acyl-ACP synthetase activity** J. Biol. Chem., 276 (38) (2001), pp. 35934-35939
[27] H. Schulz **On the structure–function relationship of acyl carrier protein of *Escherichia coli*** J. Biol. Chem., 250 (1975), pp. 2299-2304
[28] A.F. Frederick, L.E. Kay, J.H. Prestegard **Location of divalent ion sites in acyl carrier protein using relaxation perturbed 2D NMR** FEBS Lett., 238 (1) (1988), pp. 43-48
[29] R.B. Hill, K.R. MacKenzie, J.M. Flanagan, J.E. Cronan Jr., J.H. Prestegard **Overexpression, purification, and characterization of *Escherichia coli* acyl carrier protein and two mutant proteins** Protein Expr. Purif., 6 (4) (1995), pp. 394-400
[30] C.O. Rock, J.E. Cronan Jr. **Improved purification of acyl carrier protein** Anal. Biochem., 102 (2) (1980), pp. 362-364
[31] C.A. Fowler, F. Tian, H.M. Al-Hashimi, J.H. Prestegard **Rapid determination of protein folds using residual dipolar couplings** J. Mol. Biol., 304 (3) (2000), pp. 447-460
[32] D. Marion, P.C. Driscoll, L.E. Kay, P.T. Wingfield, A. Bax, A.M. Gronenborn, G.M. Clore **Overcoming the overlap problem in the assignment of 1H NMR spectra of larger proteins by use of three-dimensional heteronuclear 1H-15N Hartmann–Hahn-multiple quantum coherence and nuclear Overhauser-multiple quantum coherence spectroscopy: application to interleukin 1 beta** Biochemistry, 28 (15) (1989), pp. 6150-6156

[33] E. Zuiderweg, S. Fesik **Heteronuclear three-dimensional NMR spectroscopy of the inflammatory protein C5a** Biochemistry, 28 (1989), pp. 2387-2391
[34] J. Cavanagh, M. Rance **Sensitivity improvement in isotropic mixing (TOCSY) experiments** J. Magn. Res., 88 (1990), pp. 72-85
[35] J. Kordel, N.J. Skelton, M. Akke, A.G. Plamer, W.J. Chazin **Backbone dynamics of calcium-loaded calbindin D9k studied by two-dimensional proton-detected 15N NMR spectroscopy** Biochemistry, 31 (1992), pp. 4856-4866
[36] N.J. Skelton, A.G. Palmer, M. Akke, J. Kördel, M. Rance, W.J. Chazin **Practical aspects of two-dimensional proton-detected 15N spin relaxation measurements** J. Magn. Reson. Ser. B, 102 (1993), pp. 253-264
[37] L.E. Kay, P. Keifer, T. Saarinen **Pure absorption gradient. Enhanced heteronuclear single quantum correlation spectroscopy with improved sensitivity** J. Am. Chem. Soc., 114 (1992), pp. 10663-10665
[38] J.G. Kempf, J.P. Loria A.K. Downing (Ed.), Protein NMR Techniques, Humana Press, Totowa (2003)
[39] F. Delaglio, S. Grzesiak, G.W. Vuister, G. Zhu, J. Pfeifer, A. Bax **NMRPipe: a multidimensional spectral processing system based on UNIX pipes** J. Biomol. NMR, 6 (1995), pp. 277-293
[40] T.D. Goddard, D.G. Kneller, SPARKY 3, University of California, San Francisco.
[41] G. Lipari, A. Szabo **Model-free approach to the interpretation of nuclear magnetic resonance relaxation in macromolecules. 1. Theory and range of validity** J. Am. Chem. Soc., 104 (1982), pp. 4546-4559
[42] G. Lipari, A. Szabo **Model-free approach to the interpretation of nuclear magnetic resonance relaxation in macromolecules. 2. Analysis of experimental results** J. Am. Chem. Soc., 104 (1982), pp. 4559-4570
[43] A.M. Mandel, M. Akke, A.G. Palmer **Backbone dynamics of *Escherichia coli* ribonuclease HI: correlations with structure and function in an active enzyme** J. Mol. Biol., 246 (1) (1995), pp. 144-163
[44] R. Cole, J.P. Loria **FAST-Modelfree: a program for rapid automated analysis of solution NMR spin-relaxation data** J. Biomol. NMR, 26 (3) (2003), pp. 203-213
[45] A.G. Palmer, M. Rance, P.E. Wright **Intramolecular motions of a zinc finger DNA-binding domain from Xfin characterized by proton-detected natural abundance 13C heteronuclear NMR spectroscopy** J. Am. Chem. Soc., 113 (1991), pp. 4371-4380
[46] N. Tjandra, S.E. Feller, R.W. Pastor, A. Bax **Rotational diffusion anisotropy of human ubiquitin from ^{15}N NMR relaxation** J. Am. Chem. Soc., 117 (1995), pp. 12562-12566
[47] Y. Hiyama, C.-H. Niu, J.V. Silverton, A. Bavoso, D.A. Torchia **Determination of 15N chemical shift tensor via 15N–2H dipolar coupling in Boc-glycylglycyl [15N glycine] benzyl ester** J. Am. Chem. Soc., 110 (1988), pp. 2378-2383
[48] W.J. Fairbrother, J. Liu, P.I. Pisacane, M.X. Sliwkowski, A.G. Palmer **Backbone dynamics of the EGF-like domain of heregulin-alpha** J. Mol. Biol., 279 (5) (1998), pp. 1149-1161
[49] M. Pellecchia, P. Sebbel, U. Hermanns, K. Wuthrich, R. Glockshuber **Pilus chaperone FimC-adhesin FimH interactions mapped by TROSY-NMR** Nat. Struct. Biol., 6 (4) (1999), pp. 336-339
[50] A. Roujeinikova, C. Baldock, W.J. Simon, J. Gilroy, P.J. Baker, A.R. Stuitje, D.W. Rice, A.R. Slabas, J.B. Rafferty **X-ray crystallographic studies on butyryl-ACP reveal flexibility of the structure around a putative acyl chain binding site** Structure, 10 (2002), pp. 825-835
[51] H.C. Wong, G. Liu, Y.M. Zhang, C.O. Rock, J. Zheng **The solution structure of acyl carrier protein from *Mycobacterium tuberculosis*** J. Biol. Chem., 277 (18) (2002), pp. 15874-15880
[52] M.-M. Keating, H. Gong, D.M. Byers **Identification of a key residue in the conformational stability of acyl carrier protein** Biochem. Biophys. Acta, 1601 (2002), pp. 208-214
[53] P. Bernado, J. Garcia de la Torre, M. Pons **Interpretation of 15N NMR relaxation data of globular proteins using hydrodynamic calculations with HYDRONMR** J. Biomol. NMR, 23 (2) (2002), pp. 139-150
[54] A.M. Gehring, R.H. Lambalot, K.W. Vogel, D.G. Drueckhammer, C.T. Walsh **Ability of *Streptomyces* spp. acyl carrier proteins and coenzyme A analogs to serve as substrates in vitro for *E. coli* holo-ACP synthase** Chem. Biol., 4 (1) (1997), pp. 17-24
[55] R. Koradi, M. Billeter, K. Wuthrich **MOLMOL: a program for display and analysis of macromolecular structures** J. Mol. Graph., 14 (1) (1996), pp. 51-55